Journal of the Korean Physical Society, Vol. 71, No. 3, August 2017, pp. 171∼177

A Systematic Study of the Relationship among the Morphological, Structural and Photoelectrochemical Properties of ZnO Nanorods Grown Using the Microwave Chemical Bath Deposition Method

Sungjin Oh and Hyukhyun Ryu*
Department of Nanoscience and Engineering, High Safety Vehicle Core Technology Research Center, Inje University, Gimhae 50834, Korea

Won-Jae Lee
Department of Materials and Components Engineering, Dong-Eui University, Busan 47340, Korea

(Received 25 May 2017, in final form 1 Jun 2017)

In this study, zinc oxide (ZnO) nanostructures were grown on a ZnO seed layer/fluorine-doped tin oxide (FTO) substrate for different growth durations ranging from 5 to 40 min using the microwave chemical bath deposition method. We studied the effect of growth duration on the morphological, structural, optical and photoelectrochemical properties of the ZnO nanostructures. From this study, we found that the photoelectrochemical properties of the ZnO nanostructures were largely affected by their morphological and structural properties. As a result, we obtained the highest photocurrent density of 0.46 mA/cm^2 (at 1.5 V vs. SCE) from the sample grown for 30 min.

PACS numbers: 81.05.Dz
Keywords: ZnO nanostructures, Microwave chemical bath deposition, Growth duration, Photoelectrochemical, Photocurrent density
DOI: 10.3938/jkps.71.171

I. INTRODUCTION

Zinc oxide (ZnO) has many advantages, including high chemical, thermal and optical stability at room temperature, low material cost and low manufacturing cost [1–5]. However, most of metal-oxide materials including ZnO have poor electrical properties and short carrier lifetime. Nano-structure of metal-oxide is considered as one of strategies to overcome this problem. Various nanostructures of ZnO can be grown, such as nanoparticles [6], nanorods [7–9]. Owing to these various ZnO nanostructures, ZnO can be used in many applications, for example, in solar cells [10,11], gas sensors [3,12,13] and photoelectrochemical (PEC) cells [14–18]. PEC cells are promising devices due to their ability to produce hydrogen gas as an eco-friendly energy to replace limited fossil fuels [19–23]. Among the various ZnO nanostructures, one-dimensional (1D) ZnO structures, such as nanorods, have attracted much attention as a PEC cell photoelectrode candidate because of their high light absorption over a large surface area, superior charge transport performance due to their one-dimensional shape, enhanced interfacial reaction and reduced charge recombination on the surface [1,24–32]. The photoelectrode in the PEC cell is very important since it can affect the hydrogen gas production efficiency. Therefore, many studies currently focus on the photoelectrode [33].

There are a number of growth processes for forming photoelectrodes based on ZnO nanorods, including hydrothermal synthesis [34,35], electrochemical deposition (ECD) [36] and chemical bath deposition (CBD) [37]. Among these methods, the CBD method has the advantages of being a low-temperature, low-cost and simple method [38,39]. Recently, the microwave chemical bath deposition (MW-CBD) method, derived from the CBD process, has attracted wide interest. The MW-CBD method uses microwave energy for the process, while heat energy is used in the conventional CBD method. This microwave-assisted CBD method has many advantages, including short process time due to efficient energy transfer, very low levels of impurities, excellent reproducibility and high product yields [40–43]. Recently, ZnO growth studies using the MW-CBD method have been performed [40–42]. However, growth studies of photoelectrodes based on ZnO nanorods using the MW-CBD method are scarce. In addition, studies correlating the morphological, structural, optical and photoelectrochemical properties of ZnO nanorods grown using the MW-CBD method are also scarce.

In this work, the morphological, structural, optical

*E-mail: hhryu@inje.ac.kr; Fax: +82-55-320-3631

and photoelectrochemical properties of ZnO grown for different growth durations using the MW-CBD method were investigated, and the relationship among the morphological, structural and photoelectrochemical properties was systematically studied. Morphological properties, including surface morphology and length, and structural properties, such as preferred growth direction and crystallinity, were investigated. The morphologies of the samples were characterized using field-emission scanning electron microscopy (FE-SEM). The structural and optical properties of the ZnO nanorods were analyzed by X-ray diffraction (XRD) and ultraviolet-visible spectroscopy (UV-Vis. spectroscopy), respectively. The photoelectrochemical properties of the samples were measured using a 3-electrode potentiostat.

II. EXPERIMENTS DETAILS

In this study, a ZnO seed layer was deposited on an FTO substrate using the spin-coating method, and then ZnO nanorods were grown on the ZnO seed layer/FTO substrate for different growth durations using the MW-CBD method.

1. Cleaning the FTO substrate

The fluorine-doped tin oxide (FTO) substrates were cleaned in acetone and methanol. The cleaning methods were as follows. First, the FTO substrates were cleaned ultrasonically in acetone for 10 min, rinsed with deionized water (D.I. water) and dried under filtered air. Then, the FTO substrates were cleaned in methanol using the same methods. Next, the cleaned FTO substrates were dried at 60 °C for 10 min using an electronic oven. The dried FTO substrates were then treated for 10 min using a ulteaviolet-ozone cleaner (UVO).

2. ZnO seed layer deposited on the FTO substrate using the spin-coating method

To deposit a ZnO seed layer on the FTO substrate using the spin-coating method, a solution of 0.1 M zinc acetate dehydrate as the precursor source, 0.1 M monoethanolamine (MEA) as a stabilizer and 20 ml 2-methoxyethanol (2-ME) as the solvent was prepared. The solution was stirred at 200 revolutions per minute (rpm) at 60 °C for 3 hours, and then the solution was aged for 24 hours at room temperature. The 0.25 ml aged ZnO seed layer solution was spread on the FTO substrate using a micropipette. Then, the ZnO seed layer was deposited using spin-coating equipment at 500 rpm for 5 seconds and 4,000 rpm for 30 seconds. After spin coating, the ZnO seed layer was dried at 115 °C for 10 min. After repeating the seed layer deposition three times, the ZnO seed layer/FTO substrate was annealed at 300 °C for 5 min in Ar gas atmosphere using a rapid thermal processing (RTP) system.

3. ZnO nanostructure grown using MW-CBD

To prepare the ZnO precursor solution for MW-CBD growth, 0.05 M zinc nitrate hexahydrate and 0.05 M hexamethylenetetramine (HMT) were separately dissolved in 200 ml D.I. water with stirring at 200 rpm for 1 hour. Then, the two solutions were mixed and stirred at 200 rpm for 30 min. The prepared ZnO precursor solution was then used for the growth of ZnO nanostructures on the ZnO seed layer/FTO substrate. Different growth durations (5, 7.5, 10, 15, 20, 30 and 40 min) were examined to study the effects of growth duration on the ZnO nanostructures grown using the MW-CBD method. Post-annealing treatment was conducted at 300 °C for 1 hour in air using furnace equipment.

4. Analysis of the morphological, structural, optical and photoelectrochemical properties

The morphological properties of the ZnO nanostructures were analyzed by field-emission scanning electron microscopy (FE-SEM, Quanta 200 FEG). The structural and optical properties were analyzed by X-ray diffraction (XRD, PANalytical X'pert PRO MPD) analysis with Cu-Ka radiation and ultraviolet-visible spectroscopy (UV-Vis., SCINCO S-3100), respectively. The photoelectrochemical properties were measured using a 3-electrode potentiostat. The grown ZnO nanostructures, a graphite rod (Alfa Aesar) and a saturated calomel electrode (SCE, Sat. 3.3 M KCl) were used as the working electrode, counter electrode and reference electrode, respectively. A 300W Xenon arc lamp with 1-sun illumination (AM 1.5 filter, light intensity: 100 mW/cm^2) was used with 1 M KOH (potassium hydroxide, pH 14) as the electrolyte for conducting the photocurrent density measurements at room temperature.

III. RESULTS AND DISCUSSION

Figure 1 shows the FE-SEM images of the ZnO nanostructures grown for various growth durations using the MW-CBD method. Nanostructures were observed in all samples, including the 5 min sample, as shown in Fig. 1. The ZnO seed layer pre-deposited on the FTO substrate provides nucleation sites for the growth of ZnO nanorods. In this study, ZnO nanorods were grown over a range of durations from 5 min to 40 min. In the MW-CBD process, the precursor solution source can be decomposed

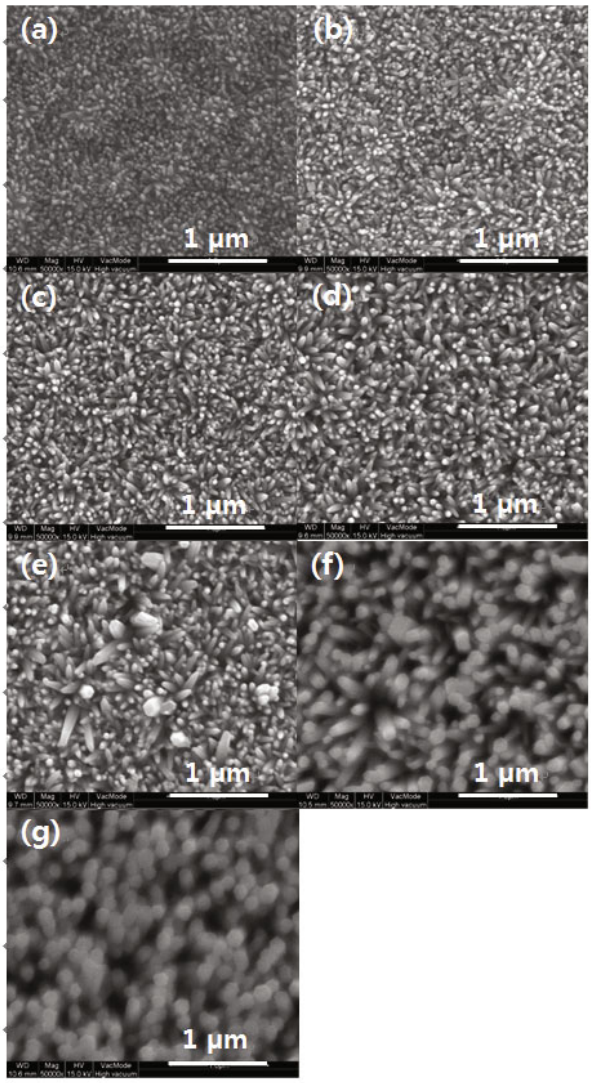

Fig. 1. Top view FE-SEM images of the ZnO nanorods with various growth durations: (a) 5, (b) 7.5, (c) 10, (d) 15, (e) 20, (f) 30 and (g) 40 min.

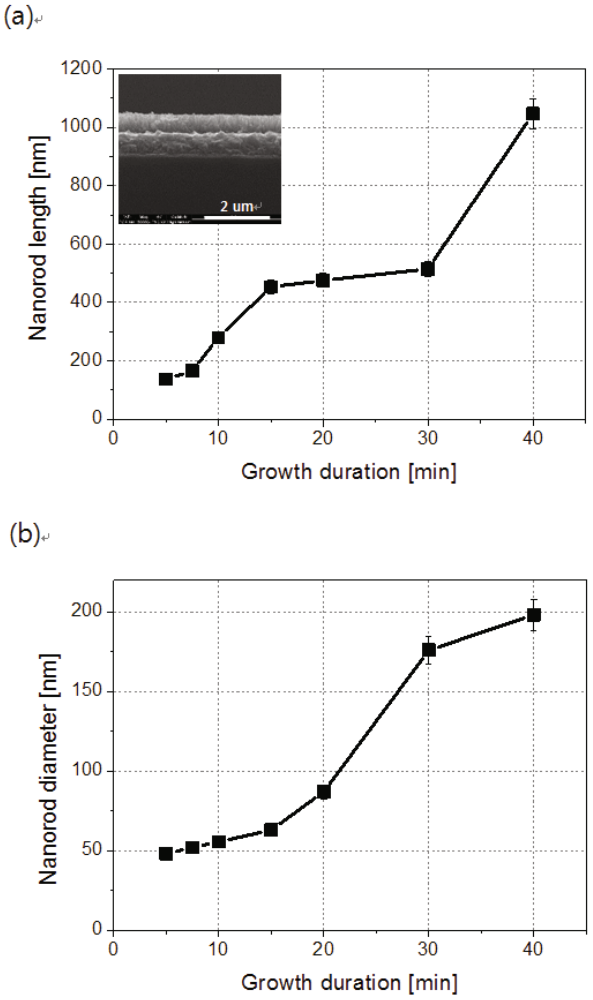

Fig. 2. (a) Nanorod length and (b) nanorod diameter of the ZnO nanorods with various growth durations.

by microwaves and become unstable, as the decomposed source can be promoted to a higher energy state. Thus, the nanorods tend to grow on the ZnO seed layer/FTO substrate through an Ostwald ripening process and then convert a stable state with lower energy [44–46].

Figure 2(a) shows length of the ZnO nanorods grown for different durations, measured from the cross-sectional SEM image. The inserted image is the cross-sectional SEM image for the 15 min grown sample. As shown in Fig. 2(a), the ZnO nanorod length increases as the growth duration increases up to 30 min and then largely increases for the 40 min sample. From Fig. 2(b), it can be seen that the nanorod diameter increases as the growth duration increases. A sharp increase in the diameter was observed from 20 to 30 min, while no substantial change in the nanorod length was found during the same growth duration range.

Figure 3 represents the X-ray diffraction results. ZnO peaks corresponding to the (002), (011) and (012) planes are found at 34.625°, 36.672° and 47.992°, respectively, and FTO substrate peaks (♦) are observed, as shown in Fig. 3(a). As the growth duration increases, it can be seen that the (002) peak intensity becomes much larger than the other ZnO peak intensities, which indicates that the (002) plane directs the vertical growth of ZnO [47]. Figure 3(b) shows the change in the (002) peak intensity over different growth durations. As the growth duration increased, the (002) peak intensity increased, and an especially large increase was found for the 40 min sample, which is possibly due to this sample having largest nanorod length and nanorod diameter in this study. In addition, with increasing growth duration, the full width at half maximum (FWHM) of the (002) peak decreased, and the grain size, calculated by Scherrer's equation [48], increased, as shown in Fig. 3(c). It is generally known that a lower FWHM implies higher crystallinity [49,50].

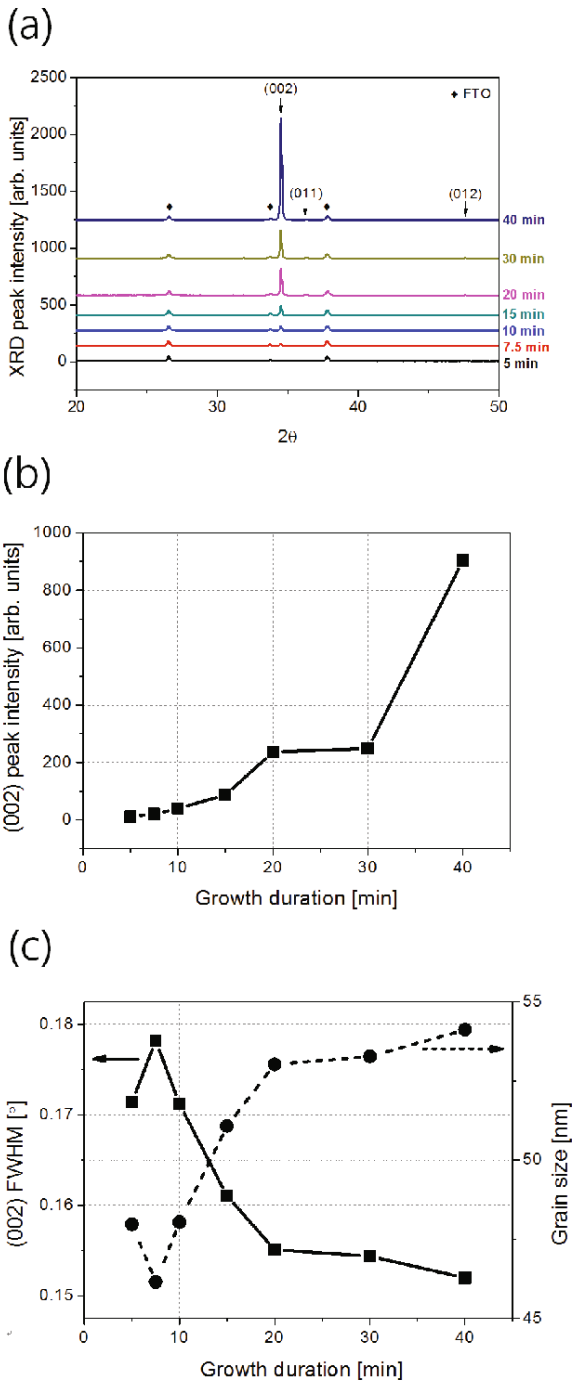

Fig. 3. (Color online) (a) XRD spectra, (b) (002) peak intensity and (c) plot of the (002) FWHM and grain size of the ZnO nanorods with various growth durations.

Therefore, it can be concluded that the crystallinity improved as the growth duration increased in this study.

The optical properties were measured using UV-Vis spectroscopy, as shown in Fig. 4. Figures 4(a) and (b) show a plot of $(\alpha h\nu)^2$ versus $h\nu$ and the optical energy bandgaps of the samples with different growth durations,

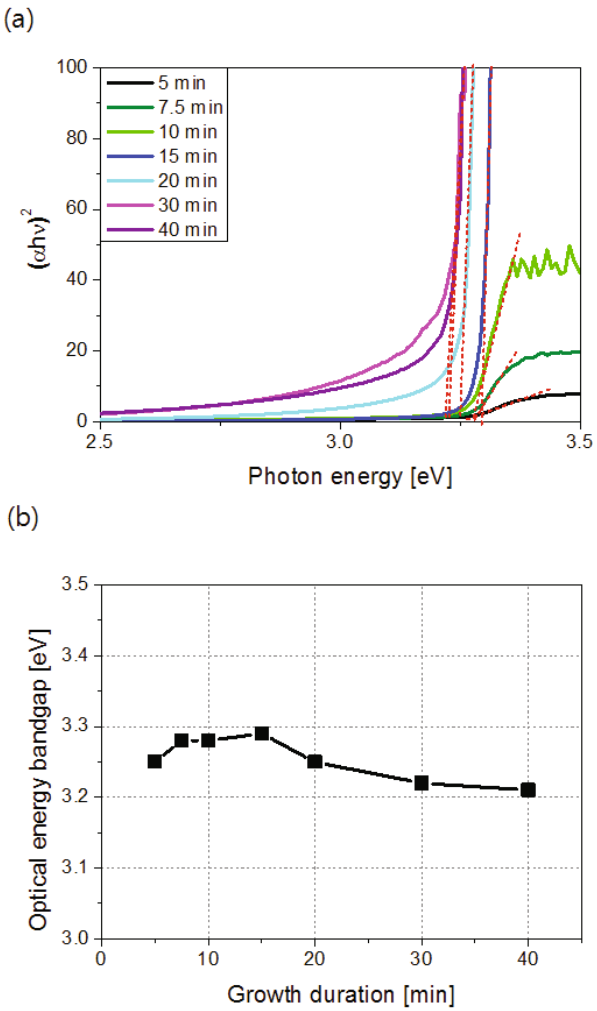

Fig. 4. (Color online) Plot of (a) $(\alpha h\nu)^2$ versus $h\nu$ and (b) the optical energy bandgap of the ZnO nanorods with various growth durations.

respectively. The optical energy bandgaps of the grown ZnO nanorods were obtained using the interaction function $(\alpha h\nu)^2 = B(h\nu - E_g)$, where α is the absorption coefficient of ZnO, $h\nu$ is the photon energy, B is a constant relative to the material, and E_g is the optical energy bandgap of ZnO [51]. In Fig. 4(b), the measured optical energy bandgaps for samples with growth durations of 5, 7.5, 10, 15, 20, 30 and 40 min were 3.25, 3.28, 3.28, 3.29, 3.25, 3.22 and 3.21 eV, respectively. These values are within the reported ZnO optical energy bandgap range of 3.2 − 3.4 eV [52].

Figure 5 shows the photoelectrochemical properties of the ZnO nanorods grown for different growth durations. Figure 5(a) shows that the current density increased with an increase in the applied potential in the positive direction, confirming the grown ZnO to be an n-type material. Additionally, it can be seen that as the growth duration increases, a relatively low dark current density is obtained, even when the applied potential is increased.

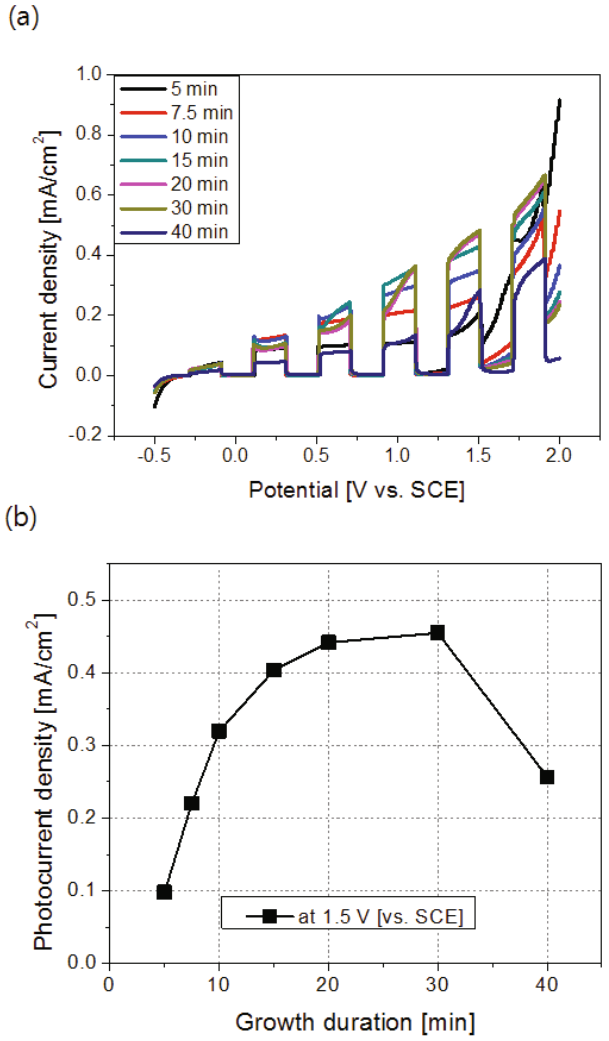

Fig. 5. (Color online) PEC performance of the ZnO nanorods with various growth durations: (a) plot of current density versus SCE and (b) the photocurrent density at 1.5 V vs. SCE.

The measured photocurrent densities under an applied potential of 1.5 V are shown in Fig. 5(b). In Fig. 5(b), the photocurrent density increases from 5 min to 30 min and then decreases at 40 min.

Figure 6 presents the relation among the morphological, structural and photoelectrochemical properties. Figures 6(a), (b), (c) and (d) show the nanorod length, the (002) XRD peak intensity, the (002) FWHM and grain size and photocurrent density for the samples with different growth durations, respectively. In Figs. 6(a) and (b), we see that the ZnO nanorod length and the (002) XRD peak intensity tend to increase with increasing growth duration. Compared to the other XRD peaks, the (002) peak intensity is significantly stronger, as discussed in Fig. 3, which indicates the c-axis-directed vertical growth of the one-dimensional ZnO nanorods [47]. The one-dimensional nanorod structure is known to have many advantages, including large surface area, high light absorption, superior transport performance, increased interface reactions and decreased recombination rate of electrons and holes, which can the improve the photocurrent density [24–32]. In Figs. 6(a), (c) and (d), the photocurrent density tends to increase with increasing ZnO nanorod length and grain size over the growth duration of 5 to 30 min. A similar result has been reported in which the photocurrent density increased with increased nanorod length [53]. In addition, the photocurrent density is also known to increase with increasing grain size due to the reduction in the electron-hole pair recombination rate with a decrease in the grain boundary density [54, 55]. As the growth duration increases, the FWHM decrease, as shown in Fig. 6(c). It can be considered that the crystallinity of the grown ZnO nanorods improves with growth duration in this study. According to previous work, improved crystallinity has a positive effect on carrier transfer and improves the photocurrent density [54]. In addition, as the growth duration increases from 5 to 40 min, the sample has a low dark current density, even at a relatively high applied potential, because carriers do not accumulate on the surface of the photoelectrode and instead smoothly escape to the electrolyte due to improved carrier transfer by the improved crystallinity of the well-grown nanorods. It is known that the dark current density of metal oxides is increased because metal oxides convert to a semi-metallic state due a reduction reaction with electrons [56, 57]. Consequently, the photocurrent density tends to increase due to improvements in the morphological and structural properties as the growth duration increases. However, even though the 40 min sample has the largest nanorod length, the highest (002) XRD peak intensity, the largest grain size, the best crystallinity and the lowest dark current density, it has a low photocurrent density of under 0.3 mA/cm^2 in this study. This result can possibly be explained by the critical length. It has been reported that if the nanorod length is longer than a critical length, the recombination rate of electron-hole pairs can increase [53,58]. Minority carriers cannot easily escape from the nanorods into the electrolyte, which results in a decrease in the photocurrent density. Therefore, it was concluded that the 40 min sample has an improper length in this study, consequently leading to a low photocurrent density. In summary, we found that the morphological and structural properties of ZnO grown using the microwave chemical bath deposition method largely affect the photoelectrochemical properties of the resultant ZnO nanorods.

IV. CONCLUSION

In this study, zinc oxide (ZnO) nanostructures were grown on a ZnO seed layer/fluorine-doped tin oxide

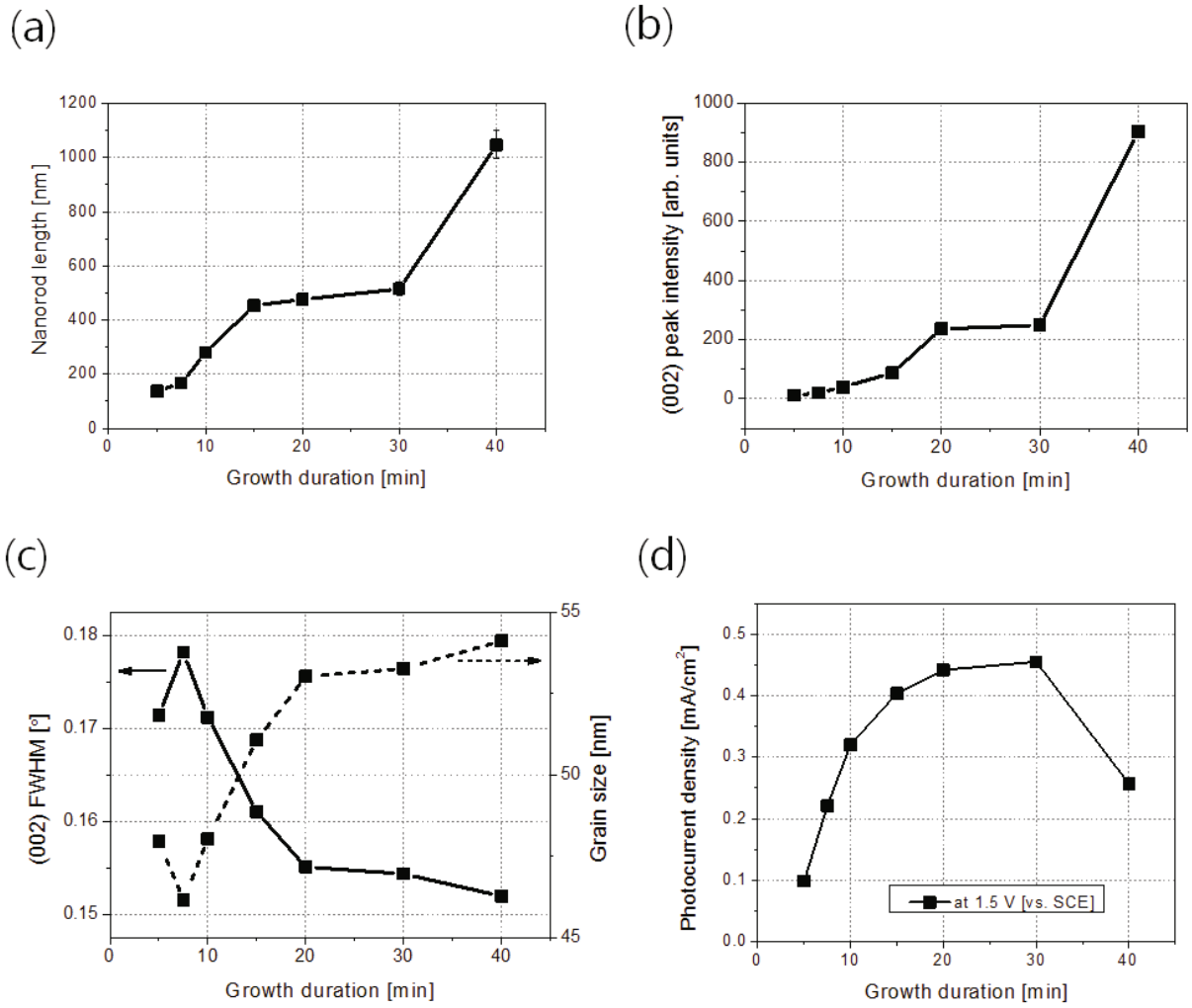

Fig. 6. Correlation among the morphological, structural and PEC properties of the ZnO nanorods with various growth durations: (a) nanorod length, (b) (002) peak intensity, (c) (002) FWHM and (d) photocurrent density.

(FTO) substrate for growth durations of 5, 7.5, 10, 15, 20, 30 and 40 min using the microwave chemical bath deposition method (MW-CBD). The morphological, structural, optical and photoelectrochemical properties of the grown ZnO samples were investigated, and the relationship among the morphological, structural and photoelectrochemical properties was systematically studied. As the growth duration increased, the nanorod length, the (002) peak intensity and the grain size increased, and the crystallinity improved. That is, the morphological and structural properties improved with growth duration, resulting in an improvement in the photocurrent density. However, the 40 min sample shows a low photocurrent density, possibly due to the excessive ZnO nanorod length. In this study, we showed that the photoelectrochemical properties are closely related to the morphological and structural properties of ZnO nanostructures grown using MW-CBD.

ACKNOWLEDGMENTS

This research was supported by Basic Science Research Program through the National Research Foundation of Korea (NRF) funded by the Ministry of Education (NRF-2016R1D1A3B01008959).

REFERENCES

[1] L. Wang, Y. Kang, X. Liu, S. Zhang, W. Huang and S. Wang, Sens. Actuators B **162**, 237 (2012).
[2] W. Han, L. Ren, X. Qi, Y. Liu, X. Wei, Z. Huang and J. Zhong, Appl. Surf. Sci. **299**, 12 (2014).
[3] J. Chen, J. Li, J. Li, G. Xiao and X. Yang, J. Alloys Compd. **509**, 740 (2011).
[4] J. Jang and H. Ryu, J. Nanoelectron. Optoelectron. **9**, 107 (2014).
[5] Z. L. Wang, ACS Nano **2**, 1987 (2008).

[6] W. Tu, J. Lei, P. Wang and H. Ju, Chem. Eur. J. **17**, 9440 (2011).
[7] M. Guo, P. Diao and S. Cai, Appl. Surf. Sci. **249**, 71 (2005).
[8] J. J. Hassan, Z. Hassan and H. Abu-Hassan, J. Alloys Compd. **509**, 6711 (2011).
[9] L. L. Yang, Q. X. Zhao and M. Willander, J. Alloys Compd. **469**, 623 (2009).
[10] A. Belaidi, T. Dittrich, D. Kieven, J. Tornow, K. Schwarzburg and M. Lux-steiner, Phys. Stat. Sol. (RRL) **2**, 172 (2008).
[11] E. Galoppini, J. Rochford, H. Chen, G. Saraf, Y. Lu, A. Hagfeldt and G. Boschloo, J. Phys. Chem. B **110**, 16159 (2006).
[12] T. Gao and T. H. Wang, Appl. Phys. A **80**, 1451 (2005).
[13] O. Lupan, V. V. Ursaki, G. Chai, L. Chow, G. A. Emelchenko, I. M. Tiginyanu, A. N. Gruzintsev and A. N. Redkin, Sens. Actuators B **144**, 56 (2010).
[14] H. Li, Y. Fu, H. Liu, M. Zhu, Z. Peng, J. Yang, J. Li, X. Huang, Y. Jiang, Q. Liu, X. Shi, H. Wu, Y. Yang and Q. Liu, Inorg. Chem. Commun. **30**, 182 (2013).
[15] M. Gupta, V. Sharma, J. Shrivastava, A. Solanki, A. P. Singh, V. R. Satsangi, S. Dass and R. Shrivastav, Bull. Mater. Sci. **32**, 23 (2009).
[16] Y. Qiu, K. Yan, H. Deng and S. Yang, Nano Lett. **12**, 407 (2012).
[17] C. Hsu and D. Chen, Int. J. Hydrogen Energy **36**, 15538 (2011).
[18] K. Ahn, S. Shet, T. Deutsch, C, Jiang, Y. Yan, M. Al-Jassim and J. Turner, J. Power Sources **176**, 387 (2008).
[19] A. Ikaram, S. Sahai, S. Rai, S. Dass, R. Shrivastav and V. R. Satsangi, J. Power Sources **267**, 664 (2014).
[20] T. Bak, J. Nowotny, M. Rekas and C. C. Sorrell, Int. J. Hydrogen Energy **27**, 991 (2002).
[21] M. Gratzel, Nature **414**, 338 (2001).
[22] J. Nowotny, C. C. Sorrell, T. Bak and L. R. Sheppard, Solar Energy **78**, 593 (2005).
[23] Y. S. Chaudhary, A. Agrawal, R. Shrivastav, V. R. Satsangi and S. Dass, Int. J. Hydrogen Energy **29**, 131 (2004).
[24] H. Oh, H. Ryu and W. Lee, J. Alloys Compd. **620**, 55 (2015).
[25] M. Fekete, W. Ludwig, S. Gledhill, J. Chen, A. Patti and L. Spiccia, Eur. J. Inorg. Chem. **2014**, 750 (2014).
[26] S. Anandan, X. Wen and S. Yang, Mater. Chem. Phys. **93**, 35 (2005).
[27] L. Liu, K. Hong, T. Hu and M. Xu, J. Alloys Compd. **511**, 195 (2012).
[28] W. Zhang, L. Jiang and J. Ye, J. Phys. Chem. C **113**, 16247 (2009).
[29] E. Garnett and P. Yang, Nano Lett. **10**, 1082 (2010).
[30] Y. J. Hwang, C. Hahn, B. Liu and P. Yang, ACS Nano **6**, 5060 (2012).
[31] X. Feng, K. Shankar, O. K. Varghese, M. Paulose, T. J. Latempa and C. A. Grimes, Nano Lett. **8**, 3781 (2008).
[32] M. Liu, N. L. Snapp and H. Park, Chem. Sci. **2**, 80 (2011).
[33] V. M. Aroutiounian, V. M. Arakelyan and G. E. Shahnazaryan, Solar Energy **78**, 581 (2005).
[34] Z. Qin, Q. Liao, Y. Huang, L. Tang, X. Zhang and Y. Zhang, Mater. Chem. Phys. **123**, 811 (2010).
[35] Y. Bu, Z. Chen, W. Li and J. Yu, ACS Appl. Mater. Interfaces **5**, 5097 (2013).
[36] C. Yao, B. Wei, H. Ma, H. Ii, L. Meng, X. Zhang and Q. Gong, J. Power Sources **237**, 295 (2013).
[37] T. H. Jeon, S. K. Choi, H. W. Jeong, S. Kim and H. Park, J. Electrochem. Sci. Technol. **2**, 187 (2011).
[38] R. Shabannia, Prog. Nat. Sci.: Mater. Int. **25**, 95 (2015).
[39] O. F. Farhat, M. M. Halim, M. J. Abdullah, M. K. M. Ali and N. K. Allam, Beilstein J. Nanotechnol. **6**, 720 (2015).
[40] A. M. Peiro, J. A. Ayllon, J. Peral, X. Domenech and C. Domingo, J. Cryst. Growth **285**, 6 (2005).
[41] A. Kothari and T. K. Chaudhuri, Mater. Lett. **65**, 847 (2011).
[42] K. Ocakoglu, Sh. A. Mansour, S. Yildirimcan, A. A. Al-Ghandi, F. El-Tantawy and F. Yakuphanoglu, Spectrochim. Acta Part A: Mol. Biomol. Spectrosc. **148**, 362 (2015).
[43] C. Wu, C. Shiau, D. W. Ayele, W. Su, M. Cheng, C. Chiu and B. Hwang, Chem. Mater. **22**, 4185 (2010).
[44] A. Phuruangrat, T. Thongtem and S. Thongtem, Mater. Lett. **63**, 1224 (2009).
[45] X. Hu, J. C. Yu, J. Gong, Q. Li and G. Li, Adv. Mater. **19**, 2324 (2007).
[46] M. Tsuji, M. Hashimoto, Y. Nishizawa, M. Kubokawa and T. Tsuji, Chem. Eur. J. **11**, 440 (2005).
[47] O. Lupan, L. Chow, G. Chai, B. Roldan, A. Naitabdi, A. Schulte and H. Heinrich, Mater. Sci. Eng. B **145**, 57 (2007).
[48] K. Ishikawa, K. Yoshikawa and N. Okada, Phys. Rev. B **37**, 5852 (1988).
[49] A. K. Kercher and D. C. Nagle, Carbon **41**, 15 (2003).
[50] F. Tsunesada, T. Iwai, T. Watanabe, H. Adachi, M. Yoshimura, Y. Mori and T. Sasaki, J. Cryst. Growth **237**, 2104 (2002).
[51] O. Lupan, T. Pauporte, L. Chow, B. Viana, F. Pelle, L. K. Ono, B. R. Cuenya and H. Heinrich, Appl. Surf. Sci. **256**, 1895 (2010).
[52] A. Dhara, B. Show, A. Baral, S. Chabri, A. Sinha, N. R. Bandyopadhyay and N. Mukherjee, Sol. Energy **136**, 327 (2016).
[53] W. Chiu, C. Lee, H. Cheng, H. Lin, S. Liao, J. Wu and W. Hsieh, Energy Environ. Sci. **2**, 694 (2009).
[54] Y. Hsu, S. Lee, J. Chang, C. Tseng, K. Lee and C. Wang, Int. J. Electrochem. Sci. **8**, 11615 (2013).
[55] S. J. Hong, H. Jun, P. H. Borse and J. S. Lee, Int. J. Hydrogen Energy **34**, 3234 (2009).
[56] C. Li, Y. Li and J. Delaunay, ACS Appl. Mater. Interfaces **6**, 480 (2014).
[57] A. Walsh, K. Ahn, S. Shet, M. N. Huda, T. G. Deutsch, H. Wang, J. A. Turner, S. Wei, Y. Yan and M. M. Al-Jassim, Energy Environ. Sci. **2**, 774 (2009).
[58] T. Hamamura, J. T. Dy, K. Tamaki, J. Nakazaki, S. Uchida, Y. Kubo and H. Segawa, Phys. Chem. Chem. Phys. **16**, 4551 (2014).